aurum

AURUM MÜHENDİSLİK SİSTEMLERİ VE MİMARLIK DERGİSİ
AURUM JOURNAL OF ENGINEERING SYSTEMS AND ARCHITECTURE

Cilt 8, Sayı 2 | Kış 2024
Volume 8, No 2 | Winter 2024

COUPLED ELECTRICAL-THERMAL ANALYSIS OF LIGHTNING DIRECT EFFECT ON AIRCRAFT COMPOSITE STRUCTURES

Mehmet PEKTAŞ[1,3*], Serkan KURT[1,3], Özkan ALTAY[3]
[1]Department of Electronic and Communication Engineering, Yildiz Technical University, Turkiye,
mehmet.pektas@std.yildiz.edu.tr
(https://orcid.org/0009-0004-5054-4791)
[2]Department of Electronic and Communication Engineering, Yildiz Technical University, Turkiye,
skurt@yildiz.edu.tr
(https://orcid.org/0000-0003-0769-0991)
[3]Turkish Aerospace Industries, Turkiye,
ozaltay@tai.com.tr
(https://orcid.org/0000-0002-8109-7961)

Received: 04.06.2004
Accepted: 04.06.2024
Published: 31.12.2024
*Corresponding author

Research Article
pp.187-197

DOI: 10.53600/ajesa.1495200

Abstract

In this study, the damage caused by the lightning direct effect on carbon fiber reinforced polymer (CFRP) aircraft structures located in the initial lightning strike zones has been addressed. Lightning current component A was applied to both CFRP and copper foil coated CFRP models, and coupled electrical-thermal analyses were conducted using the finite element method implemented in the Abaqus software. The analysis aimed to investigate the effectiveness of 448 g/m² solid copper foil in reducing the damage caused by Joule heating, one of the direct effects of lightning, in CFRP, as well as to determine the influence of panel size variation on the extent of damage.

Keywords: lightning, direct effect, aircraft, electrical-thermal analysis, CFRP

HAVA ARACI KOMPOZİT YAPILARINDA YILDIRIMIN DOĞRUDAN ETKİSİNİN BAĞLI ELEKTRİK-TERMAL ANALİZİ

Özet

Bu çalışmada, yıldırımın ilk temas bölgelerinde bulunan karbon fiber takviyeli polimer (KFTP) hava aracı yapılarında yıldırımın doğrudan etkisi ele alınmıştır. KFTP ve bakır folyo kaplanmış KFRP modellerine yıldırım akım komponenti A uygulanarak sonlu elemanlar yöntemini kullanan Abaqus yazılımı ile bağlı elektriksel termal analizler gerçekleştirilmiştir. Analiz ile yıldırımın doğrudan etkilerinden biri olan joule ısısının neden olduğu KFTP'deki hasar miktarının azaltılmasında 448 g/m² bakır folyonun etkinliği ve panel boyutu değişiminin hasar miktarı üzerindeki etkisi ortaya koyulmuştur.

Anahtar Kelimeler: yıldırım, doğrudan etki, hava aracı, elektrik-termal analiz, KFTP

1. Introduction

The formation of lightning occurs when the electric field generated by electric charges in clouds reaches a sufficient intensity, resulting in the ionization of the air. Lightning can occur in three forms: cloud-to-ground, cloud-to-cloud, and intra-cloud. According to statistical studies based on reported lightning strike incidents, commercial aircraft are exposed to lightning strikes approximately once every 3000 flight hours, or once a year (B. Fisher, Taeuber, & Crouch, 1988; F. A. Fisher & Plumer, 1977). For F-4 aircraft flying in Europe, 10.5 lightning strikes per 10,000 flight hours have been reported (F. A. Fisher & Plumer, 1977). Considering these rates, the probability of lightning strikes varies regionally, posing a significant safety threat to aircraft. Lightning has two distinct effects on aircraft, direct and indirect. This study focuses on the direct effect of lightning on aircraft.

In today's aviation, the use of metals in structural components of aircraft is being replaced by carbon fiber reinforced polymers (CFRP) introduced by modern technology. This transition is primarily driven by the pursuit of weight reduction in aircraft structures, thereby increasing payload capacity. However, the low electrical and thermal conductivities of CFRPs render them susceptible to structural damage when subjected to electromagnetic environmental effects such as lightning strikes. Joule heating (ohmic heating), one of the direct effects of lightning, plays a significant role in causing damage in CFRP structures, particularly through delamination. Due to Joule heating, the carbon fibers in the CFRP begin to sublimate at temperatures above 3000°C (Ogasawara, Hirano, & Yoshimura, 2010), and the resin binding the carbon fibers burns and undergoes pyrolysis at temperatures above 350°C (Plumer & Robb, 1982). Consequently, the layers disintegrate, leading to a loss of structural integrity.

To protect aircraft from the direct effects of lightning, it is essential to first analyze the aircraft's lightning strike zones. The magnitude and waveforms of the lightning current to which aircraft structures will be exposed vary according to the lightning strike zones. When designing aircraft structural components, the zones where the component will be subjected to lightning strikes are taken into consideration. Particularly for structures like CFRP, metal foils with high conductivity are embedded in the topmost layer to protect them from lightning. The high conductivity of the metal foil provides minimization of damage to CFRP resulting from Joule heating.

2. Lightning Aircraft Interaction

In 10% of lightning strike cases involving aircraft, the aircraft is struck by an approaching lightning leader, while in 90% of cases, the aircraft triggers the formation of lightning (Larsson, 2002). The lightning channel tends to attach to specific points on the aircraft. Since the aircraft moves at a certain speed relative to the lightning channel during a lightning strike, the lightning channel sweep over the aircraft as shown in Figure 1. Due to the different current amplitudes and waveforms of subsequent lightning strikes following the initial lightning strike, the aircraft is divided into lightning strike zones.

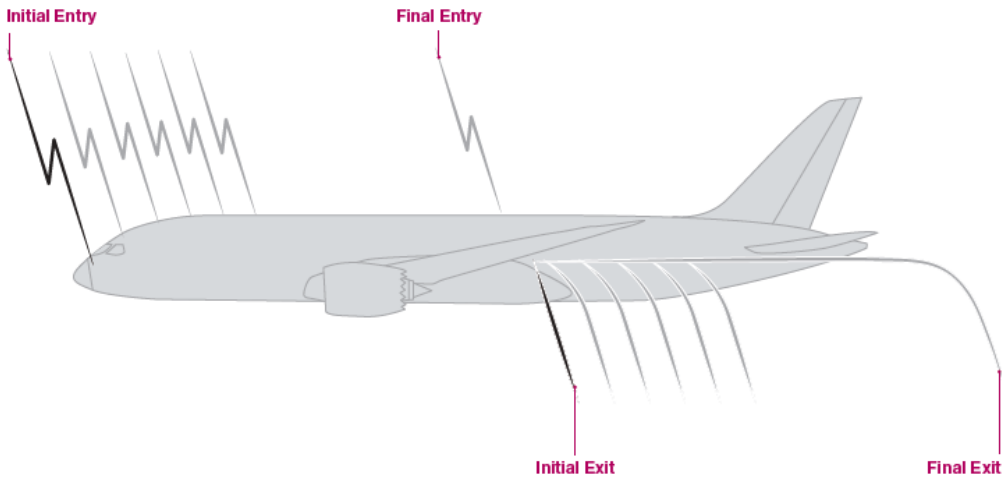

Figure 1. Swept channel attachment points on aircraft (Sweers, Birch, & Gokcen, 2012).

2.1. Aircraft Lightning Strike Zones

Lightning strike zones are fundamentally divided into three sections. The first zones are the parts where the first lightning attachment occurs and are exposed to the first return stroke. The second zones are the parts subjected to subsequent return strokes due to the sweeping of the lightning channel as a result of the aircraft's cruising speed. The third zones are the areas where there is no direct lightning attachment but conduct the lightning current (SAE ARP5414B, 2018).

In Figure 2 below, the results of the electrical field analysis for the F-16 model are presented. The analysis was conducted using the electrostatic solver of the CST program. The CAD model of the F-16 is sourced from (Yağmur, H. (2020). Regions with high electric field concentration on the surface of the F-16, which is charged with 1 Coulomb, can be observed. These regions represent the initial attachment points of the lightning strike.

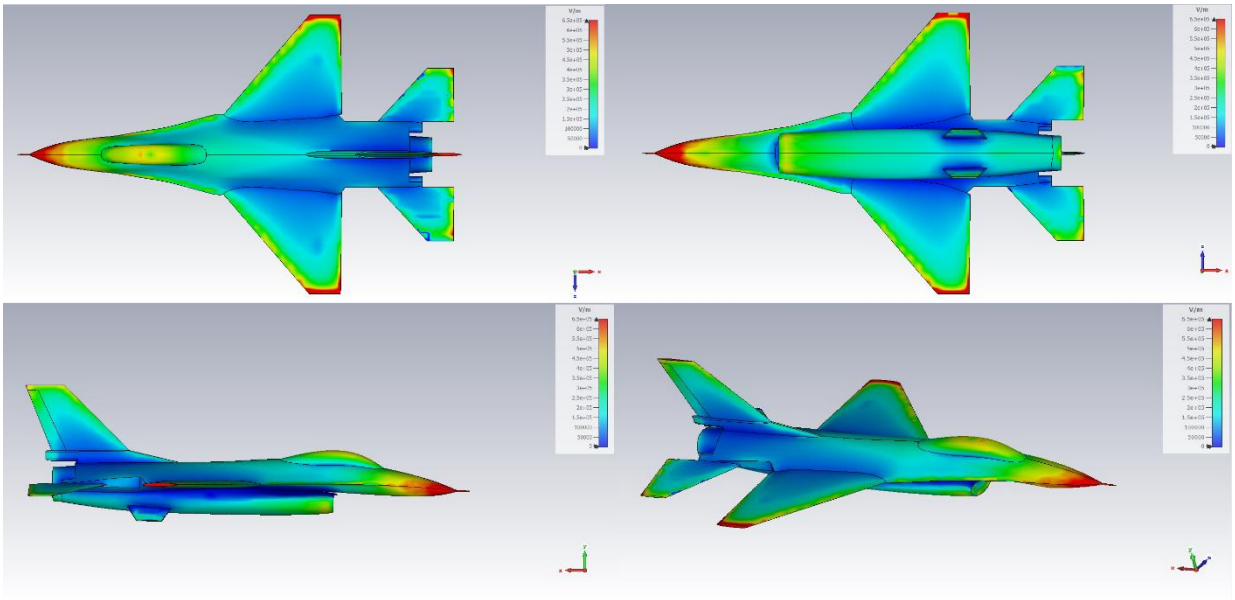

Figure 2. F-16 lightning attachment analysis results.

2.2. Lightning Current Waveforms

(SAE ARP5412B, 2013) defines the lightning current waveforms to which the aircraft will be exposed based on the lightning strike zones. These waveforms are classified into four types: lightning current components A, B, C, and D.

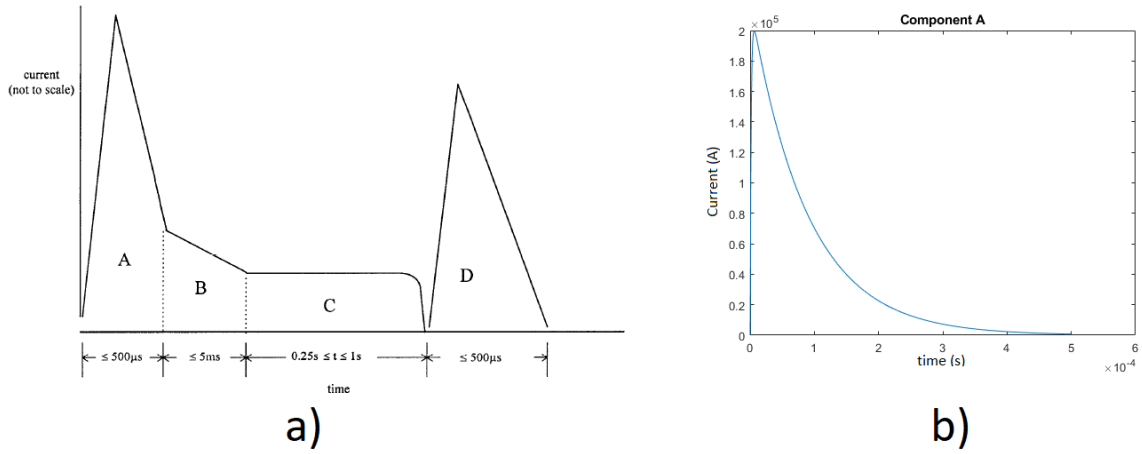

Figure 3. a) Lightning current waveforms b) Lightning current component A

(SAE ARP5412B, 2013) specifies that current components A, B, and C must be applied sequentially for the lightning strike zone 1A test. This is because the impact of current components on damage is related not only to their own waveform parameters but also to the changes induced in the structure by the preceding current component (Sun, Yao, Xu, Chen, & Wu, 2019).

Studies indicate that the primary cause of damage in CFRP resulting from lightning strikes is attributed to transient current components (Karch & Metzner, 2016; Karch, Heidler, & Paul, 2021). Current component A induces Joule heating in CFRP, leading to damage and various mechanical forces (Karch, Heidler, & Paul, 2021). Therefore, the analysis will utilize the A current component, as shown in Figure 3b."

Current component A is mathematically defined by the exponential expression given in Equation (1) (SAE ARP5412B, 2013).

$$I(t) = I_0(e^{-\alpha t} - e^{-\beta t})(1 - e^{-\gamma t})^2 \qquad (1)$$

I_0 = 218810 A

α = 11354 s^{-1}

β = 647265 s^{-1}

γ = 5423540 s^{-1}

t = time (s)

3. Coupled Electrical-Thermal Analysis

The coupled electrical-thermal analyses were performed using the Abaqus software, which employs the finite element method. In the analysis, the electrical potential of the specimen exposed to the lightning current is calculated under specified electrical boundary conditions. Subsequently, a transient heat transfer analysis is conducted by applying Joule heating to each finite element under certain thermal boundary conditions. During the analysis, the temperature-dependent electrical conductivity is taken into account, thus ensuring full coupling between the electrical and thermal analyses. The theoretical foundation of the analysis is briefly outlined below (Hibbitt, Karlsson, & Sorensen, 1997).

The conservation of charge for a control volume V with surface S is defined as follows:

$$\int_S J.n\, dS = \int_V r_c\, dV \tag{2}$$

J is the electric current density per unit area, n is the outward normal to the surface, and r_c is the internal volumetric current source per unit volume.

Using the definition of the electric field, Ohm's law can be expressed as follows:

$$J = \sigma E = -\sigma \nabla \varphi \tag{3}$$

E is the electric field intensity, σ is the electrical conductivity, and φ is the electric potential. This equation assumes that the electrical conductivity is independent of the electric field.

The fundamental equation for electrical analysis is obtained by combining Ohm's law with the charge conservation equation.

$$\int_V \delta\varphi \nabla.(\sigma \nabla \varphi) dV = \int_V \delta\varphi r_c dV + \int_S \delta\varphi J.n dS \tag{4}$$

The Joule's law defines the electrical energy dissipated (P_{ec}) from a current-carrying conductor.

$$P_{ec} = J.E = (\sigma E).E \tag{5}$$

The equation for heat conduction analysis is defined by the fundamental energy balance relationship.

$$\int_V \rho C_v \frac{\partial \theta}{\partial t} \delta\theta dV + \int_V \delta\theta \nabla.(k \nabla \theta) dV = \int_V \delta\theta r dV + \int_S \delta\theta q.n dS \tag{6}$$

θ is the temperature, k is the thermal conductivity, ρ is the density, C_v is the specific heat, r is the heat generation rate, and q is the heat flux density directed into the control volume.

The Abaqus software discretizes these equations using the finite element method and solves them iteratively. The electric potential, electric current, Joule heating, and temperature of each element is calculated.

3.1. Finite Element Analysis Model

For the analysis, CFRP panels and CFRP panels embedded with copper foil, each measuring 500 mm x 50 0mm and 250 mm x 250 mm, respectively, have been modeled. The CFRP consists of 28 layers, each with a thickness of 184 µm. The copper foil used in the top layer has a thickness of 50 µm, corresponding to 448 g/m². The total thickness for the CFRP model is 5.152 mm, whereas for the copper foil coated CFRP model, the thickness is 5.202 mm. In the analysis, the lightning current component A, as depicted in Figure 3b, is applied at the exact center point of the specimens' upper surface, with the specimens being grounded from their lateral sides. The initial temperature is 25°C. The thermal emissivity of CFRP is taken as 0.9, while that of copper is 0.03. Temperature-dependent material properties are provided in Tables 1 and 2.

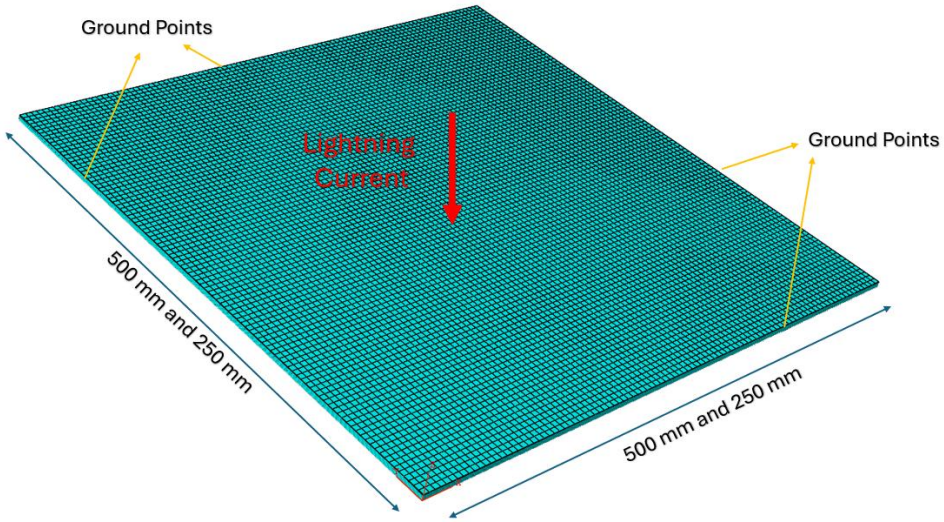

Figure 4. FEA model of specimens.

Table 1 Temperature-Dependent Material Properties of CFRP (Guo et al., 2017).

Temperature $(°C)$	Density (kg/m^3)	Specific Heat $(J/(kg.K))$	Longitudinal Thermal Conductivity $(W/(m.K)$	Transverse/ In-depth Thermal Conductivity $(W/(m.K)$	Longitudinal Electrical Conductivity (S/m)	Transverse Electrical Conductivity (S/m)	In-depth Electrical Conductivity (S/m)
25	1520	1065	11.8	0.609	2.93E+04	77.8	7.94E-04
300	1520	2100	11.8	0.609	2.93E+04	77.8	7.94E-04
400	1520	2100	2.608	0.18	2.93E+04	778	7.94
500	1100	2100	1.736	0.1	2.93E+04	2.00E+03	2.00E+03
600	1100	1700	1.736	0.1	2.93E+04	2.00E+03	2.00E+03
1000	1100	1900	1.736	0.1	2.93E+04	2.00E+03	2.00E+03
3316	1100	2509	1.376	0.1	2.93E+04	2.00E+04	2.00E+04
>3316	1100	5875	1.00E+08	1.00E+08	1.00E+08	1.00E+08	1.00E+08

Table 2 Temperature-Dependent Material Properties of Copper (Li et al., 2020).

Temperature ($°C$)	Density (kg/m^3)	Specific Heat ($J/(kg.K)$)	Thermal Conductivity (W/$(m.K)$	Electrical Conductivity (S/m)
25	8950	385	401	58140000
500	8500	431	370	20120000
510	8490	431	339	4651000
1000	7945	490.952	150	3704000
2562	7600	490.952	180	2227000
>2562	7600	550	180	1.00E+08

3.2. Analysis Results

The resin in CFRP begins to decompose at 300°C and fully melts and pyrolyzes at 500°C, while carbon fibers start to sublime at 3000°C (Ogasawara, Hirano, & Yoshimura, 2010). Therefore, in evaluating the analysis results, it will be assumed that the resin is damaged at temperatures of 300°C and above, and the carbon fibers are damaged at temperatures of 3000°C and above.

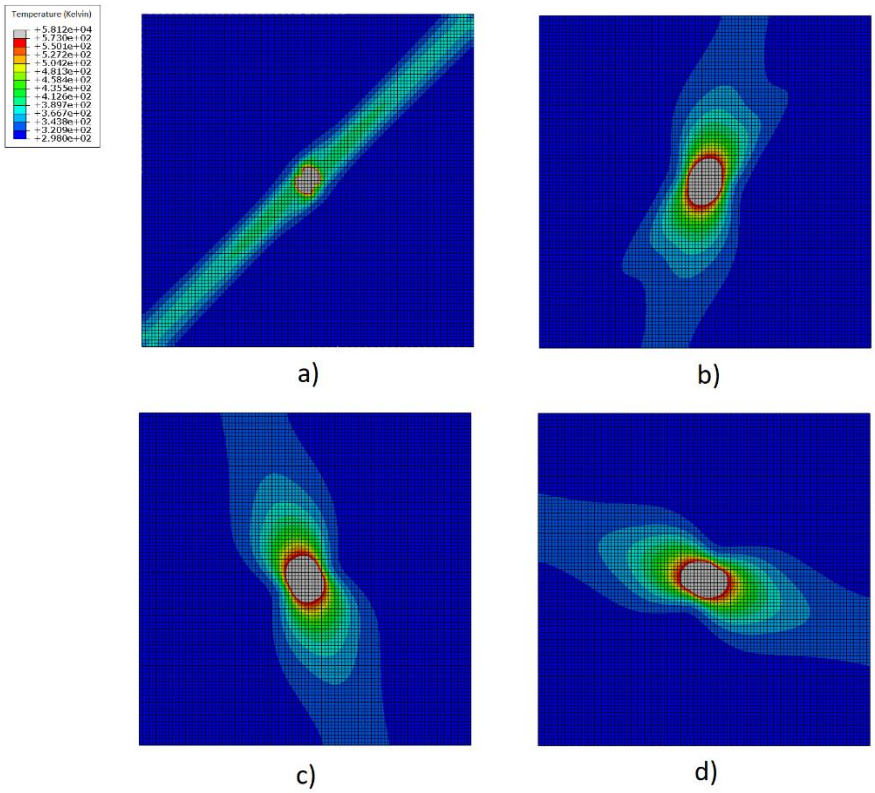

Figure 5. Temperatures of the first four layers of the 500 mm x 500 mm CFRP model: a) first layer (45°); b) second layer (90°); c) third layer (-45°); d) fourth layer (0°).

Due to the anisotropic material properties of the layers constituting the CFRP and the different orientations of these layers, the area of temperature distribution varies across each layer, as seen in Figure 5. The orientation angle of each layer in the CFRP plays a significant role in the damage area on the specimen.

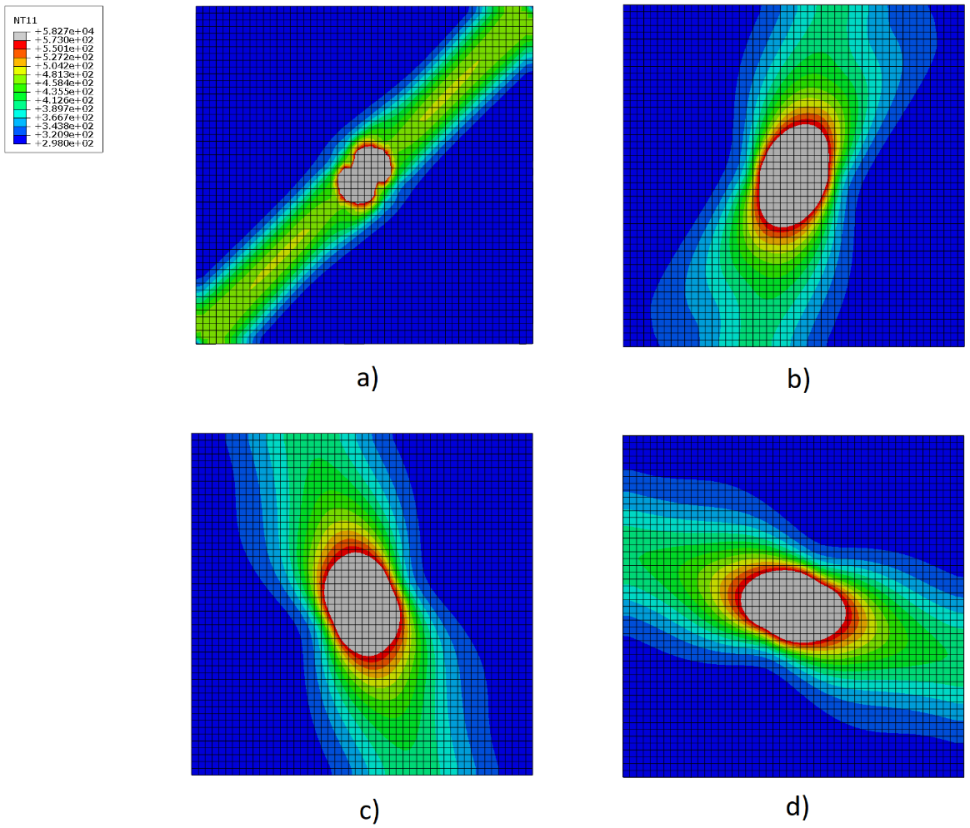

Figure 6. Temperatures of the first four layers of the 250 mm x 250 mm CFRP model: a) first layer (45°); b) second layer (90°); c) third layer (-45°); d) fourth layer (0°).

When the dimensions of the CFRP model are changed, as seen in Figure x, there is a slight increase in temperature only in the first layer oriented at 45 degrees. Nevertheless, the extent of the damage area remains unchanged.

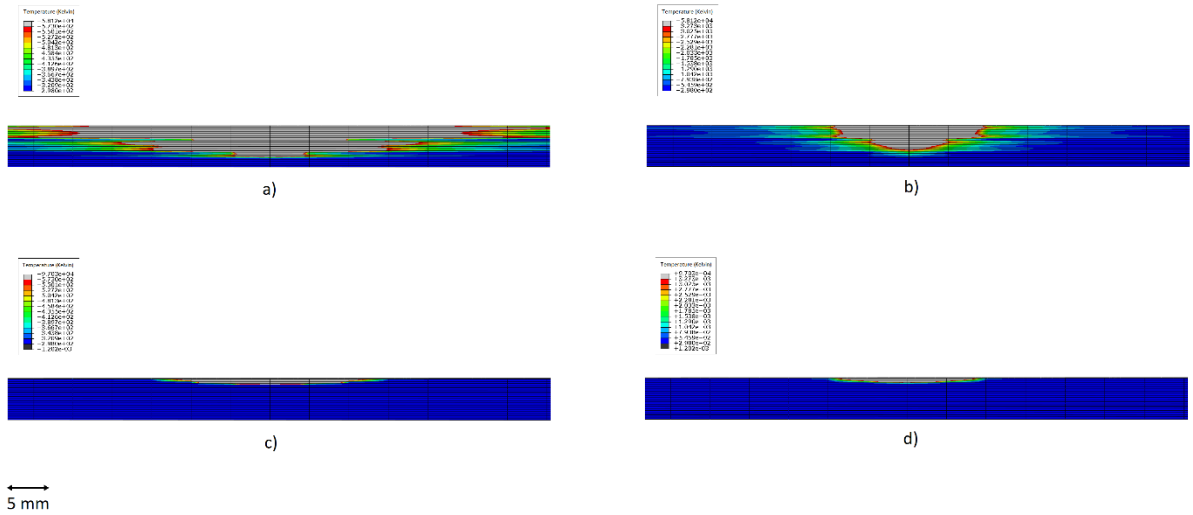

Figure 7. The temperature distributions in the thickness direction of the 500 mm x 500 mm CFRP and Copper foil coated CFRP models: a) CFRP model up to 300°C; b) CFRP model up to 3000°C; c) Copper foil coated CFRP model up to 300°C; d) Copper foil coated CFRP model up to 3000°C.

In the CFRP model, temperature values of 300°C are observed up to the 21st layer, while temperature values of 3000°C are observed up to the 17th layer. Resin has vaporized up to a depth of 3.864 mm, while carbon fibers have sublimated up to a depth of 3.128 mm. Damage has occurred in the sample up to a depth of 3.864 mm. In the copper foil coated CFRP model, temperature values of 300°C are observed up to the 4th layer, and temperature values of 3000°C are observed up to the 3rd layer. Resin has vaporized up to a depth of 0.736 mm, while carbon fibers have sublimated up to a depth of 0.552 mm. Damage has occurred in the panel up to a depth of 0.736 mm.

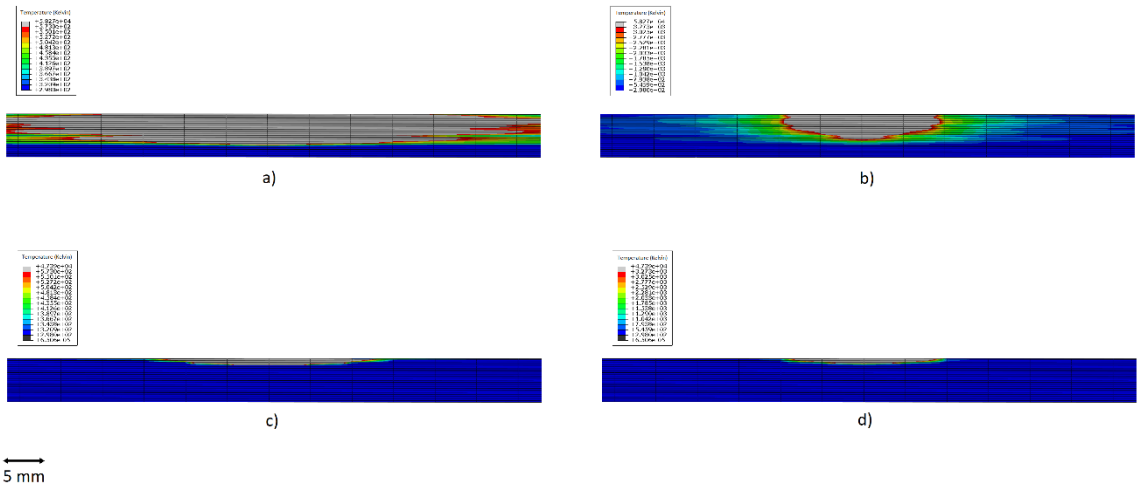

Figure 8. The temperature distributions in the thickness direction of the 250 mm x 250 mm CFRP and Copper foil coated CFRP models: a) CFRP model up to 300°C; b) CFRP model up to 3000°C; c) Copper foil coated CFRP model up to 300°C; d) Copper foil coated CFRP model up to 3000°C.

As seen in Figure 8, when the dimensions of the CFRP and copper foil coated CFRP models changed, the depth of damage caused by the resin decreased by one layer in the CFRP model. However, in the copper foil coated CFRP model, no significant difference in damage depth was observed.

4. Conclusion

Despite the size differences of 250 mm x 250 mm and 500 mm x 500 mm in the specimens, no significant differences in either depth or area damage caused by Joule heating were observed. When 448 g/m² copper foil was applied to the surface of the CFRP, the depth damage caused by Joule heating decreased from 3.864 mm to 0.736 mm. The primer coating and paint on the top layer of composite structures were not considered in the analyses. Given the low conductivity of these materials, it is expected that the damage resulting from lightning tests would be greater than the damage predicted by the analysis. Additionally, copper coating and carbon fibers cannot contribute to electrical current conduction and heat transfer above certain temperatures due to their sublimation. This will lead to differences between the test results and the analysis results. While the direct effects of lightning cannot be fully modeled, coupled electrical-thermal analyses can reveal differences arising from various factors such as different types of materials, coatings, or dimensional variations.

ACKNOWLEDGEMENTS

This study was supported by Turkish Aerospace Industries.

References

Fisher, B., Taeuber, R., & Crouch, K. (1988). Implications of a recent lightning strike to a NASA jet trainer. 26th Aerospace Sciences Meeting. https://doi.org/10.2514/6.1988-394ZPorter, M. E. (1998).

Fisher, F. A., & Plumer, J. A. (1977, April 1). Lightning protection of aircraft. Retrieved from https://ntrs.nasa.gov/citations/19780003081

Guo, Y., Dong, Q., Chen, J., Yao, X., Yi, X., & Jia, Y. (2017). Comparison between temperature and pyrolysis dependent models to evaluate the lightning strike damage of carbon fiber composite laminates. Composites. Part a, Applied Science and Manufacturing, 97, 10–18. https://doi.org/10.1016/j.compositesa.2017.02.022

Hibbitt, Karlsson, & Sorensen. (1997). ABAQUS: Theory manual (Vol. 2).

Karch, C., Heidler, F., & Paul, C. (2021). Protection of Aircraft Radomes against Direct Lightning Strikes—An Overview. Atmosphere, 12(9), 1141. https://doi.org/10.3390/atmos12091141

Karch, C., & Metzner, C. (2016, September). Lightning protection of carbon fibre reinforced plastics — An overview. https://doi.org/10.1109/iclp.2016.7791441

Larsson, A. (2002). The interaction between a lightning flash and an aircraft in flight. Comptes Rendus. Physique, 3(10), 1423–1444. https://doi.org/10.1016/s1631-0705(02)01410-x

Li, B., Chang, F., Xiao, Y., Wei, X., He, W., & Ming, Y. (2020). Thermal Ablation Damage Analysis of CFRP Suffering from Lightning Based on Principles of Tomography. Materials, 13(22), 5159. https://doi.org/10.3390/ma13225159

Ogasawara, T., Hirano, Y., & Yoshimura, A. (2010). Coupled thermal–electrical analysis for carbon fiber/epoxy composites exposed to simulated lightning current. Composites. Part a, Applied Science and Manufacturing, 41(8), 973–981. https://doi.org/10.1016/j.compositesa.2010.04.001

Plumer, J., & Robb, J. (1982). The direct effects of lightning on aircraft. IEEE Transactions on Electromagnetic Compatibility, EMC-24(2), 158–172. https://doi.org/10.1109/temc.1982.304010

SAE ARP5412B. (2013). SAE International. https://doi.org/10.4271/ARP5412B

SAE ARP5414B. (2018). SAE International. https://doi.org/10.4271/ARP5414B

Sun, J., Yao, X., Xu, W., Chen, J., & Wu, Y. (2019). Evaluation method for lightning damage of carbon fiber reinforced polymers subjected to multiple lightning strikes with different combinations of current components. Journal of Composite Materials, 54(1), 111–125. https://doi.org/10.1177/0021998319860562

Sweers, G., Birch, B., & Gokcen, J. (2012). Lightning strikes: protection, inspection, and repair. Aero Magazine, 4(2012), 19-28.

Yağmur, H. (2020). F-16 Fighting Falcon. Grabcad. https://grabcad.com/library/f-16-fighting-falcon-4